ADVANCED ELECTRONIC MATERIALS Open Access
www.advelectronicmat.de

Superconductivity and Pronounced Electron-Phonon Coupling in Rock-Salt $Al_{1-x}O_{1-x}$ and $Ti_{1-x}O_{1-x}$

Pjotrs Žguns, Nuh Gedik, Bilge Yildiz, and Ju Li**

The highest ambient-pressure Tc among binary compounds is 40 K (MgB2). Higher Tc is achieved in high-pressure hydrides or multielement cuprates. Alternatively, are explored superconducting properties of binary, metastable sub-oxides, that may emerge under extremely low oxygen partial pressure. The emphasis is on the rock-salt structure, which is known to promote superconductivity, and exploring AlO, ScO, TiO, and NbO. Dynamic lattice stability is achieved by introducing metal and oxygen vacancies in the fashion of $Nb_{1-x}O_{1-x}$-type structure (x = ¼). The electron-phonon (e-ph) coupling is remarkably large in $Al_{1-x}O_{1-x}$ and $Ti_{1-x}O_{1-x}$ ($\lambda \approx 2$ at x = ¼), with Tc ≈ 35 K according to the Allen–Dynes equation. Significantly, the coupling strength is comparable to that in high-pressure hydrides, yet, in contrast to hydrides and MgB2, the coupling is largely driven by low frequency phonons. $Sc_{1-x}O_{1-x}$ and $Nb_{1-x}O_{1-x}$ show significantly smaller λ and Tc. Further, hydrogen intercalation to boost λ and Tc is investigated. Only $Ti_{1-x}(O_{1-x}Hx)$ and $Nb_{1-x}(O_{1-x}Hx)$ are dynamically stable upon intercalation, where H, respectively, decreases and increases Tc. The effect of H doping on electronic structure and Tc is discussed. Altogether, the study suggests that metal sub-oxides are promising compounds to achieve strong e-ph coupling at ambient pressure.

1. Introduction

Superconductors are used in key technologies such as strong magnets for medical imaging and maglev trains, the lossless transmission of electricity, quantum computing, etc. Attaining high critical temperature T_c is desirable to bring operation conditions closer to ambient and reduce cooling costs.

The T_c had long been considered to have an upper bound of ≈20 K (the so-called Matthias limit,[1,2] and also Cohen–Anderson limit[3,4]), with Nb_3Ge alloy holding the record $T_c \sim 23$ K[5,6] until the discovery of unconventional cuprate superconductors with $T_c \sim 30$ K in 1986[7] that then grew to ≈130 K by 1993.[8] However, conventional superconductors, those obeying the Bardeen–Cooper–Schrieffer (BCS) theory,[9] were mostly within the expected limit. The discovery of MgB_2 conventional superconductor with $T_c \sim 39$ K (2001)[10] sparked enthusiasm to find materials with a higher T_c among the BCS superconductors.

In contrast to unconventional superconductors, the strategies to achieve high T_c in the BCS superconductors are generally well understood. The pioneering work of Ashcroft[11,12] suggested employing exotic (far from ambient) conditions such as extreme pressure, to achieve the metallic phase of hydrogen[11] and metal hydrides[12] where T_c would be driven by high-frequency phonons of the light element and strong e-ph coupling. Recent developments of crystal structure prediction algorithms and first-principles calculations of e-ph coupling allowed the identification of superconducting phases and prediction of their T_c, most notably predicting H_3S[13,14] and LaH_{10},[15,16] with their superconducting properties and T_cs on the order of 200 K confirmed experimentally.[17,18]

Superconducting phases may also be promoted by exotic chemical conditions such as the increased chemical potential of species (e.g., exceptionally high or low oxygen partial pressure P_{O2} or gas atmosphere different from ambient). Recently, Palnichenko and co-workers reported superconducting-like behavior in various metal-oxygen systems such as Na/NaO_x,[19] Mg/MgO_x,[20] Al/AlO_x,[21] Fe/FeO_x,[22] Cu/CuO_x,[23] Mo/MoO_{3-x},[24] Bi/Bi_2O_3.[25] These systems were often obtained by high-temperature oxidation of metals or reduction of oxides, and although superconductivity was often volatile and filamentary, the reported T_c was high, typically on the order of 50 K or even up to 120 K (Fe/FeO_x[22]). Superconducting behavior was also reported in the Bi_2O_3-based memristor device with Bi filaments.[26] In all these examples, metal-oxygen

P. Žguns, B. Yildiz, J. Li
Department of Materials Science and Engineering
Massachusetts Institute of Technology
77 Massachusetts Avenue, Cambridge, MA 02139–4307, USA
E-mail: byildiz@mit.edu; liju@mit.edu
N. Gedik
Department of Physics
77 Massachusetts Avenue, Cambridge, MA 02139–4307, USA
B. Yildiz, J. Li
Department of Nuclear Science and Engineering
Massachusetts Institute of Technology
77 Massachusetts Avenue, Cambridge, MA 02139–4307, USA

The ORCID identification number(s) for the author(s) of this article can be found under https://doi.org/10.1002/aelm.202400141

DOI: 10.1002/aelm.202400141

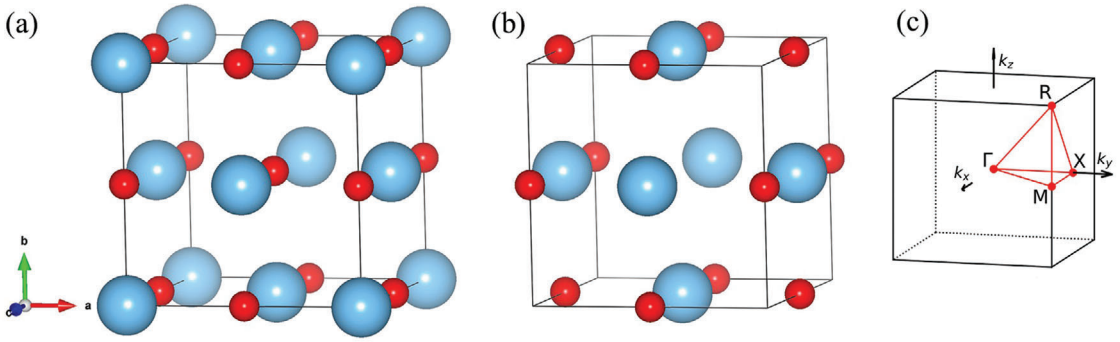

Figure 1. a) Conventional unit cell of rock-salt (B1) structure M_1O_1 (*cP8*, *Fm-3m*). b) Conventional unit cell of $M_{1-x}O_{1-x}$ ($x = ¼$, *cP6*, *Pm-3m*). It can be seen as a B1 structure with two vacancies at (0, 0, 0) and (½, ½, ½) sites, as known for NbO.[38] c) Brillouin zone of the *cP* unit cell; high-symmetry paths are shown in red. Color code for atoms in a) and b): M is blue, O is red.

phases or stoichiometries far from conventional may emerge, potentially giving rise to a high T_c. Meta-stable compounds were long anticipated to deliver high-T_c superconductivity,[5] and these experimental findings motivate us to search among the metal-oxygen phases. Identifying such compounds can help us eventually stabilize or synthesize them by means of ampoule or vacuum furnace-based crystal growth,[27] or far-from-equilibrium techniques such as plasma treatment,[28] or epitaxial film growth[29–31] with lattice-matching substrates, which may be more feasible than applying extreme pressure.

In this work, we search for meta-stable compounds that may emerge under extremely reducing or oxidizing conditions and exhibit high T_c. Since there are many plausible phases of metal oxides, we start with the structure types that are known to promote superconductivity in a variety of chemistries and evaluate their T_c in the BCS framework. One such archetypal structure is the rock-salt structure (B1, **Figure 1a**), and several transition metal nitrides and carbides were reported to have a high T_c up to 20–30 K.[32,33] Therefore, we consider the metal oxides in the B1 phase to find out if they could have a strong e-ph coupling and a high T_c. We are further motivated by the fact that $T_c = 5$ K was recently reported in LaO rock-salt oxide,[30] and 5.5 K[27] and 7.4 K[29] in TiO were reported recently after improvements in the synthesis procedures, which leaves room for achieving high T_c in this class of sub-oxide compounds where the metal cation valence is lower than their typical values on the surface of Earth.

Particularly, we explore rock-salt AlO, ScO, TiO, and NbO intermetallic compounds. These oxides have metallic electronic structures (see, e.g., the Materials Project database[34]), allowing us to predict their T_c within the BCS framework. Recently, the T_c of metallic LaO was determined within the BCS framework,[35] matching well with the experimental records,[30] which is reassuring for our approach. Moreover, Sc, Ti and Nb sequence allows us to explore the periodic trend (we substitute V for Nb since VO has a band gap[34,36]). The ideal, vacancy-free structure of these oxides is thermodynamically and dynamically unstable (i.e., possesses imaginary frequency and is not stable with respect to lattice vibrations). $Ti_{1-x}O_{1-x}$ has vacancies ($x = 0.15$) that stabilize the structure; $Al_{1-x}O_{1-x}$ is reported for high temperature only;[37] NbO oxide has 25% of vacancies on both oxygen and metal sites, i.e., $Nb_{1-x}O_{1-x}$ ($x = ¼$).[38] We chose to study these compounds in the form of NbO-type structure (see Figure 1b), which remedies phononic instabilities and makes these compounds dynamically stable. For the chosen oxides, we perform electronic structure and lattice dynamics calculations, confirming that these compounds are metallic in their normal state and are dynamically stable. We carry out e-ph calculations and employ Wannier interpolation techniques to accurately compute Eliashberg spectral function and e-ph coupling strength, and T_c. Next, we consider the effect of H intercalation and its effect on the electronic structure, dynamics, and e-ph coupling, and T_c. We find that these binary oxides with NbO-type structure can manifest strong e-ph coupling, as observed for $Al_{1-x}O_{1-x}$ ($\lambda = 2.1$) and $Ti_{1-x}O_{1-x}$ ($\lambda = 1.8$). The strength of e-ph coupling is comparable to that reported for high-pressure, high-T_c hydrides, and is driven primarily by acoustic phonons which now all have positive stiffness. The resultant T_c reaches up to 36 K and is higher than that reported[32,33] in rock-salt nitrides and carbides.

2. Results and Discussion

T_c is calculated by following the Allen–Dynes equation with modified $f_\omega f_\mu$ prefactors that correct predictions for high T_c superconductors:[39]

$$T^{ML}{}_c = \frac{f_\omega f_\mu \omega_{log}}{1.20} \exp\left(-\frac{1.04\,(1+\lambda)}{\lambda - \mu^*\,(1+0.62\lambda)}\right) \quad (1)$$

μ^* was set to 0.10 in our results. We note there are three factors in equation (1): the exponential factor $\exp(-\frac{1.04(1+\lambda)}{\lambda-\mu^*(1+0.62\lambda)})$ that depends on e-ph coupling strength λ, the ω_{log} prefactor, and the $f_\omega f_\mu$ prefactor (see Methods for the definition of these parameters).

2.1. $Al_{1-x}O_{1-x}$, $Sc_{1-x}O_{1-x}$, $Ti_{1-x}O_{1-x}$, $Nb_{1-x}O_{1-x}$

Rock-salt Al_1O_1, Sc_1O_1, Ti_1O_1, and Nb_1O_1 compounds are thermodynamically unstable. Their convex hull energies, E_{hull}, range from 0.1 eV/atom to 1.3 eV/atom (see the Materials Project[34,40] data provided in Table S1, Supporting Information). Moreover, our phonon calculations show that three of these compounds are dynamically unstable (Al_1O_1, Ti_1O_1, Nb_1O_1). This is expected

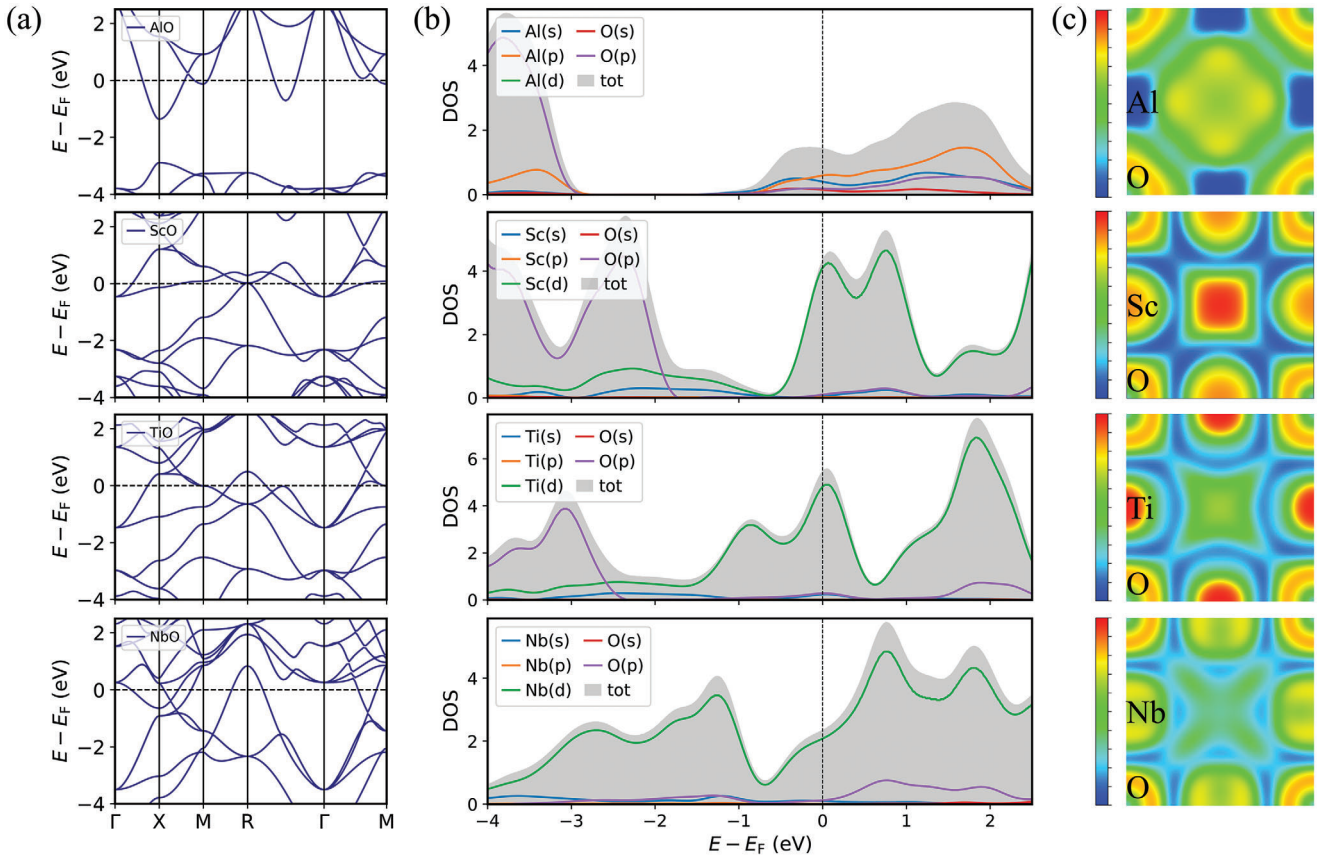

Figure 2. Electronic structure of $Al_{1-x}O_{1-x}$, $Sc_{1-x}O_{1-x}$, $Ti_{1-x}O_{1-x}$, $Nb_{1-x}O_{1-x}$ ($x = ¼$, *cP*6, NbO-type structure): a) Band structure. b) Projected DOS. c) Electron localization function colormap of the [002] plane (the vacant oxygen site is in the center). The colormap spans values from 0 (blue) to 1 (red), indicating delocalization and strong localization, respectively. E_F is the Fermi level.

since Al monoxide is unstable at room temperature,[37] while Ti monoxide possesses ≈15% of (disordered) Ti and O vacancies ($Ti_{0.85}O_{0.85}$),[41–43] and Nb monoxide possesses 25% of ordered vacancies ($Nb_{0.75}O_{0.75}$).[38] Likewise, theoretical studies of Ti_1O_1 report the appearance of imaginary phonons that can be cured by the introduction of Ti and O vacancies.[44] We show that the introduction of vacancies in the fashion of the NbO-type structure ($x = ¼$)[38] makes Al, Ti, and Nb monoxides significantly more stable, with E_{hull} decreasing by 0.2...0.8 eV/atom (see Table S1, Supporting Information; though, only $Nb_{0.75}O_{0.75}$ is thermodynamically stable). Most importantly, all four oxides are dynamically stable in the NbO-type structure, and we therefore used it in further calculations.

Band structure calculations show that $Al_{1-x}O_{1-x}$, $Sc_{1-x}O_{1-x}$, $Ti_{1-x}O_{1-x}$, and $Nb_{1-x}O_{1-x}$ are metallic (**Figure 2**a), which agrees with the experimental report of metallic conduction in Ti and Nb monoxides.[43] In $Al_{1-x}O_{1-x}$, the valence band at the Fermi level is dominated by Al 3p and 3s states, with the contribution of O 2p and 2s states (Figure 2b). In $Sc_{1-x}O_{1-x}$, $Ti_{1-x}O_{1-x}$ and $Nb_{1-x}O_{1-x}$, the Fermi level is dominated by d states, with only marginal contribution of O 2p and other states (Figure 2b). Electron localization function[45] analysis suggest that these oxides have metallic bonding character especially in between the sites (Figure 2c), with some strong localization of electrons close to Ti in $Ti_{1-x}O_{1-x}$ and in the oxygen vacancy in $Sc_{1-x}O_{1-x}$ (Figure 2c).

All four oxides are dynamically stable in the NbO-type phase, as mentioned above; no imaginary frequencies are present (**Figure 3**). However, phonon softening is seen in the dispersion: Thus, $Al_{1-x}O_{1-x}$ has significant softening of acoustic modes along the Γ−X and Γ−M paths, indicating proximity to dynamical instability. Indeed, this phase is highly unstable (E_{hull} = 0.768 eV/atom, Table S1, Supporting Information). These acoustic branches (Γ−X and Γ−M) also show remarkable e-ph coupling as highlighted in Figure 3a (see Figure S1, Supporting Information for visualization of these modes). Anomalies such as dispersion wiggles are further seen at different frequency ranges, e.g., ≈25–40 meV along the M−R−Γ paths, contributing to the strong e-ph coupling (Figure 3a). In $Ti_{1-x}O_{1-x}$, the Γ−X and Γ−M acoustic branches are unusually straight. The strong e-ph coupling can be seen in Figure 3c for acoustic modes near the R and M points (see Figure S2, Supporting Information for visualization of these modes; these modes are octahedral rotations, well-known for the *Pm-3m* compounds with perovskite-like structure;[46,47] here, octahedra are Ti_6 units).

The Eliashberg spectral function and integrated e-ph coupling strength, $\lambda(\omega)$, are shown in **Figure 4**. In $Al_{1-x}O_{1-x}$, $\lambda(\omega)$ shows a steady increase and the strongest contribution comes from modes below 35 meV, with a high peak in $\alpha^2F \approx 32$ meV. Acoustic modes extend up to ≈25 meV and contribute to λ throughout their frequency range. This agrees with the fact that $Al_{1-x}O_{1-x}$

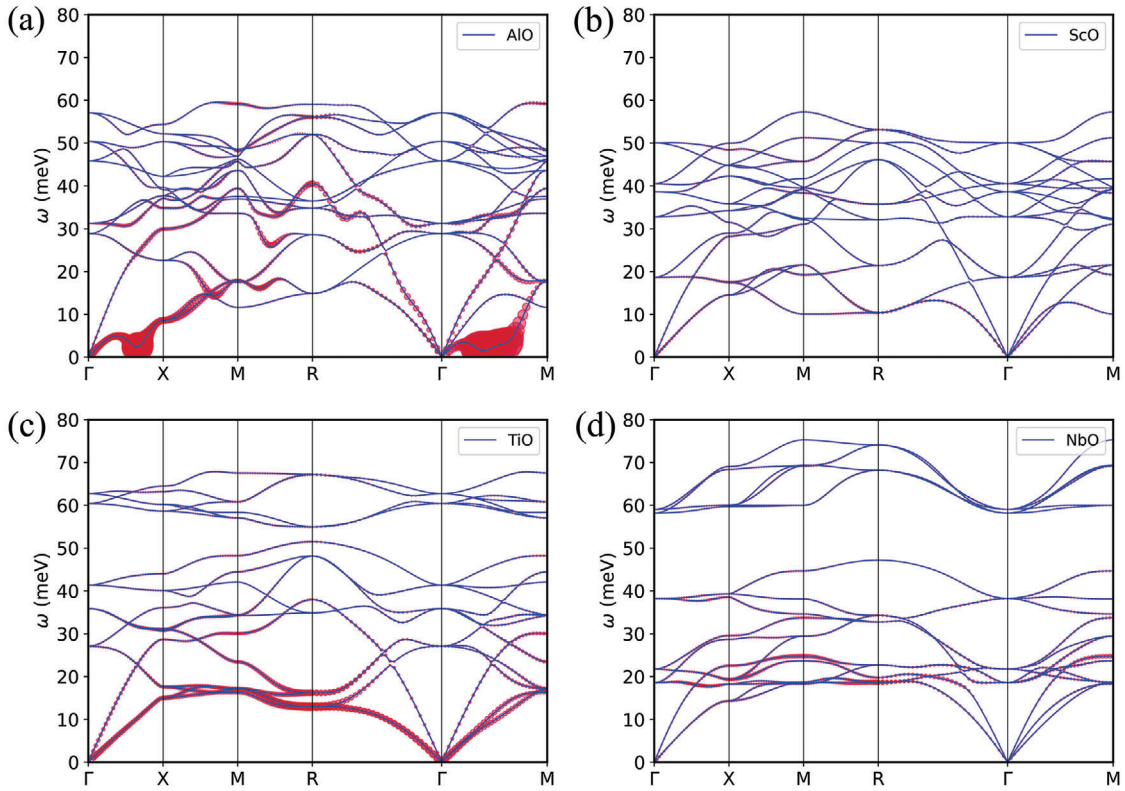

Figure 3. Phonon dispersion of a) $Al_{1-x}O_{1-x}$, b) $Sc_{1-x}O_{1-x}$, c) $Ti_{1-x}O_{1-x}$, d) $Nb_{1-x}O_{1-x}$. ($x = ¼$, *cP*6, NbO-type structure.) All compounds are dynamically stable. The e-ph coupling strength of each mode and *q*-point (λ_{qv}) is shown with red, filled circles (circle size is proportional to λ_{qv}).

has phonon anomalies of both acoustic and higher frequency modes. The integrated coupling strength is remarkably high (λ = 2.09). In $Sc_{1-x}O_{1-x}$, the e-ph coupling comes from all over the frequency range, however, the coupling is weak (λ = 0.29). In $Ti_{1-x}O_{1-x}$, the e-ph coupling is mainly driven by acoustic modes in the 10–20 meV frequency range, which constitutes ≈60% of λ. The integrated coupling is strong (λ = 1.80) and is comparable to that of $Al_{1-x}O_{1-x}$. In $Nb_{1-x}O_{1-x}$, the main contribution to λ comes from 15–25 meV acoustic phonons, however, the coupling (λ = 0.47) is weaker than that in $Ti_{1-x}O_{1-x}$. Although Sc, Ti and Nb oxides have similar electronic structures, i.e., the Fermi level is dominated by d states, the λ and respective T_c are different. This can be attributed to different electron count, which is an important factor for e-ph coupling. Indeed, the oscillatory variation of T_c along the d elements (Sc, Ti, Nb) is generally consistent with what is known for other superconductors: Thus, T_c shows oscillatory behavior with the number of valence electrons per atom in various intermetallic compounds and alloys,[48–50] as well as rock-salt transition metal carbides and nitrides as reported theoretically.[51] The electron count influences the number of bands and pockets near the Fermi level that can enhance coupling: For example, in $Ti_{1-x}O_{1-x}$, there is a nearly flat band at the Fermi level near the M point and a pocket at the Γ–M path. Furthermore, the absence of strong e-ph coupling in $Sc_{1-x}O_{1-x}$, which also have nearly flat bands close to the Fermi level, may be attributed to charge localization at the O vacancy site, as observed for only this compound (see Bader charges in Table S2, Supporting Information and strong localization at the vacancy site in Figure 2c). The charge localized at the interstitial sites is known to couple weakly with phonons and is therefore detrimental for the e-ph coupling as reported for high-pressure Li-S compounds.[52]

The summary of calculated λ and T_c is shown in **Table 1**. Intriguingly, $Al_{1-x}O_{1-x}$ and $Ti_{1-x}O_{1-x}$ show pronounced coupling ($\lambda \approx 2$), and T_c on the order of 35 K, which is relatively high for binary compounds at ambient pressure. For example, MgB_2[53] and related Li-Mg-B superconductors[54] have λ of 0.5–0.7, with the main contribution to coupling originating from high-frequency modes of Boron atoms (above 50 meV). Strong coupling on the order of $\lambda \sim 2$ was reported in high-pressure, high-T_c hydrides such as LaH_{10} (λ = 2.2 at 250 GPa) and YH_{10} (λ = 2.6

Table 1. λ, ω_{log}, and T_c^{ML} of $Al_{1-x}O_{1-x}$, $Sc_{1-x}O_{1-x}$, $Ti_{1-x}O_{1-x}$ and $Nb_{1-x}O_{1-x}$ oxides ($x = ¼$, NbO-type structure).

Compound	ω_{log} (meV)	λ	T_c^{ML} (K)
$Al_{1-x}O_{1-x}$	13.3	2.09	36
$Sc_{1-x}O_{1-x}$	0.1	0.29	0.1
$Ti_{1-x}O_{1-x}$	16.8	1.80	35
$Nb_{1-x}O_{1-x}$	25.4	0.47	2.8

Noteworthy, achieving a high T_c in the BCS superconductors depends on both the strong e-ph coupling and the ω_{log} prefactor (according to the Allen-Dynes formula.[39,63]) For example, a twofold increase of λ alone in $Al_{1-x}O_{1-x}$ would increase T_c by 37%; a two-fold increase of ω_{log} alone would increase T_c by 100% (this estimate is oversimplified since λ and ω_{log} are interdependent).

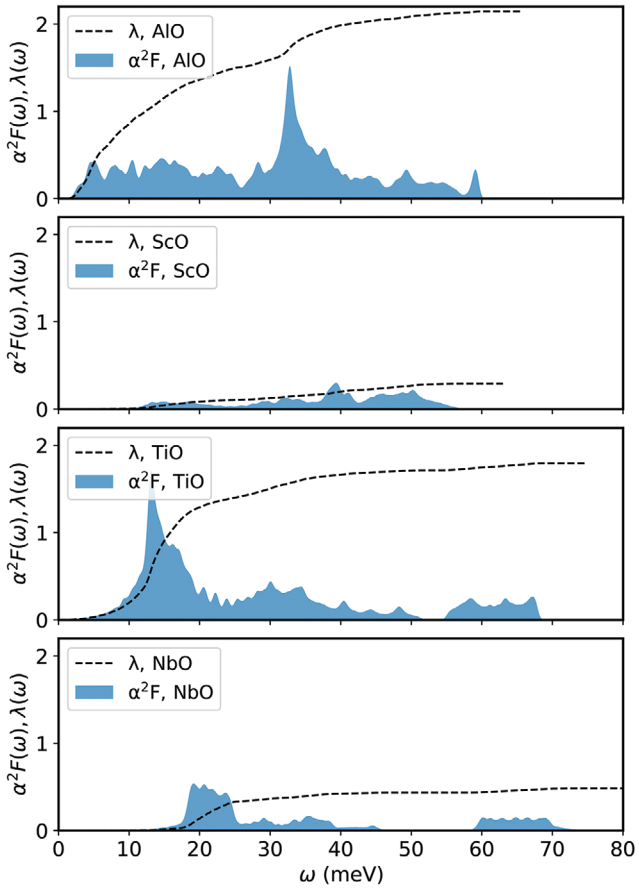

Figure 4. Eliashberg spectral function $\alpha^2F(\omega)$ and $\lambda(\omega)$ of $Al_{1-x}O_{1-x}$, $Sc_{1-x}O_{1-x}$, $Ti_{1-x}O_{1-x}$, and $Nb_{1-x}O_{1-x}$ ($x = ¼$, *cP*6, NbO-type structure).

at 250 GPa),[15] as well as H_3S ($\lambda = 2.6$ at 200 GPa),[55] and more recently in ambient-pressure meta-stable Mg_2IrH_6 ($\lambda = 2.5$ at ambient pressure).[56] However, in H_3S it originates mainly from high-frequency H modes (above 50 meV).[55] In contrast, the strong e-ph coupling in $Al_{1-x}O_{1-x}$ and $Ti_{1-x}O_{1-x}$ comes from mainly acoustic and low-frequency phonons (below 35 meV, Figure 3 and Figure 4), dominated by the metal cation participation (especially for $Ti_{1-x}O_{1-x}$, see Figure S3, Supporting Information). A strong e-ph coupling originating from low-frequency modes was recently reported in $PdCuH_x$,[57] and rock-salt transition metal carbides, namely VC, CrC, MnC and ZnC,[33] however the resultant T_c was somewhat smaller (up to 28 K in ZnC).

Few words should be said about the comparison with the available experimental and theoretical data. First, $Nb_{0.75}O_{0.75}$ is a well-known superconductor with a $T_c = 1.4$ K,[43] which is reasonably reproduced in our calculations ($T_c = 2.8$ K). The T_c of $Al_{1-x}O_{1-x}$ is not known experimentally since this compound was reported only at elevated temperatures to date.[37] For $Ti_{1-x}O_{1-x}$, the following T_c values were reported: 0.6 K,[43] 1.4 K,[58] 0.7–2.3 K,[59] and even 5.5 K[27] and 7.4 K[29] more recently. The disorder of vacancies was considered one of the plausible sources for decreasing T_c in Ti monoxide,[43] which also increases the resistance of the normal, metallic state. Previous theoretical work on TiO ($x = {}^1/_8$) has found much smaller $\lambda = 0.8$ and $T_c = 7$ K,[44] however the discrepancy might be attributed to different compositions and/or insufficient sampling of k and q points in the ref. [44] Our calculated T_c, of $Ti_{1-x}O_{1-x}$ is, however, much greater (35 K) than that previously reported in experiments. The difference can be attributed to a different composition ($x = ¼$ in our work versus $x = 0.15$ in experiments[41,42]). Further, accounting for plausible anharmonic effects may decrease the calculated T_c, as reported for AlH_3[60] and YH_6.[61] Magnetic order may also decrease the T_c,[33] which might be relevant for $Ti_{1-x}O_{1-x}$ that has slight ferromagnetic magnetization according to the MP database.[34,40] Electron correlation effects may also influence the T_c of oxides as demonstrated for bismuthate superconductors.[62]

To increase λ and ω_{log}, the introduction of H, which has a low atomic mass and high vibrational frequency, may be helpful. We therefore study it in the next section to see if it can enhance T_c through both λ and ω_{log} factors in equation (1) (for details, see Methods).

2.2. Hydrogenated Oxides: $Ti_{1-x}(O_{1-x}H_x)$, $Nb_{1-x}(O_{1-x}H_x)$

Intercalation of hydrogen in oxides with NbO-type structure can occur on either the metal or oxygen vacancy site ($x = ¼$). Our calculations show that intercalation into the metal vacancy site is energetically unfavorable (requires ≈3 eV per H atom, for $(M_{1-x}H_x)O_{1-x}$, $x = ¼$), and the obtained structures are dynamically unstable. Intercalation into the oxygen vacancy site is unfavorable for $Al_{1-x}O_{1-x}$ (1.3 eV per H atom), and favorable for $Sc_{1-x}O_{1-x}$, $Ti_{1-x}O_{1-x}$ and $Nb_{1-x}O_{1-x}$ (–0.2 eV to –0.8 eV per H, see Table S3, Supporting Information). However, $Sc_{1-x}(O_{1-x}H_x)$ is dynamically unstable, while $Ti_{1-x}(O_{1-x}H_x)$ and $Nb_{1-x}(O_{1-x}H_x)$ are dynamically stable, and we therefore investigate these two latter compounds further.

Band structure calculations show that $Ti_{1-x}(O_{1-x}H_x)$ and $Nb_{1-x}(O_{1-x}H_x)$ are metallic (**Figure 5**a). Similar to $Ti_{1-x}O_{1-x}$ and $Nb_{1-x}O_{1-x}$, the valence band at the Fermi level is dominated by d states, with only marginal contribution of O 2p and other states (Figure 5b). Electron localization function[45] analysis suggest that these oxides have metallic bonding character especially in between the sites, with some strong localization of electrons close to H atoms and Ti in $Ti_{1-x}(O_{1-x}H_x)$ (Figure 5c). The Bader charge analysis shows that hydrogen charge state is hydride anion ($q_H = -1.81\,|e|$ and $-1.68\,|e|$ in $Ti_{1-x}(O_{1-x}H_x)$ and $Nb_{1-x}(O_{1-x}H_x)$, respectively) instead of proton cation.

Both $Ti_{1-x}(O_{1-x}H_x)$ and $Nb_{1-x}(O_{1-x}H_x)$ are dynamically stable, as mentioned above; no imaginary frequencies are present (**Figure 6**). Some phonon anomalies can be seen in dispersion, e.g., the Γ–X acoustic branches in $Ti_{1-x}(O_{1-x}H_x)$ is unusually straight. The introduction of hydrogen contributes to the formation of high-frequency phonon modes at about 120 and 110 meV in $Ti_{1-x}(O_{1-x}H_x)$ and $Nb_{1-x}(O_{1-x}H_x)$, respectively. These phonon modes slightly contribute to e-ph coupling and increase the ω_{log} frequency (from 16.8 to 25.7 meV in Ti monoxide, and from 25.4 to 27.1 meV in Nb monoxide).

Significantly, the e-ph coupling in $Ti_{1-x}(O_{1-x}H_x)$ is much decreased as compared to $Ti_{1-x}O_{1-x}$. In $Ti_{1-x}(O_{1-x}H_x)$, the contribution at 10–20 meV is much smaller (**Figure 7**). The main origin of this reduction may come from the change in the electronic structure: in $Ti_{1-x}O_{1-x}$ the Fermi level crosses the bands

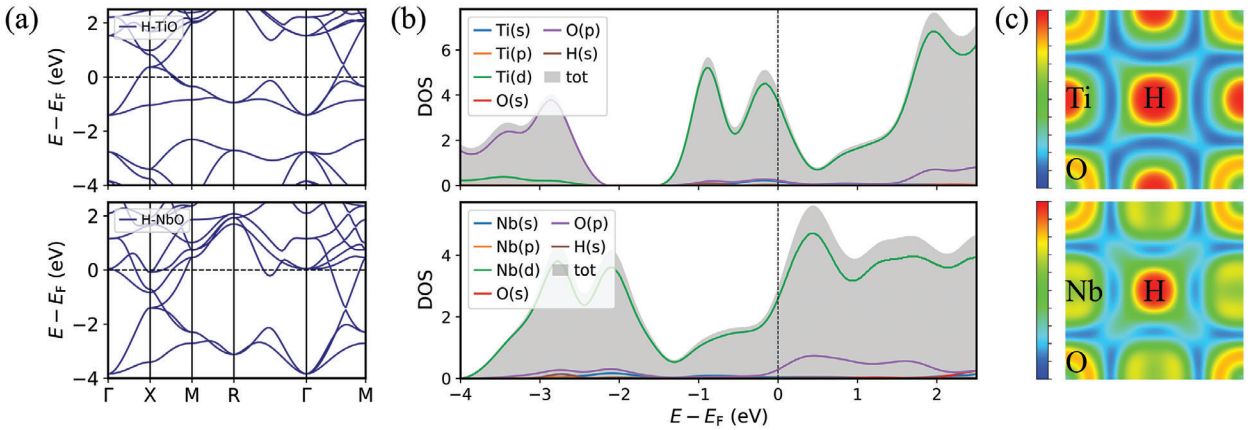

Figure 5. Electronic structure of $Ti_{1-x}(O_{1-x}H_x)$ and $Nb_{1-x}(O_{1-x}H_x)$: a) Band structure. b) Projected DOS. c) Electron localization function colormap of the [002] plane (hydrogen occupies the vacant oxygen site and is in the center of the colormap). E_F is the Fermi level.

at the Γ–M path and crosses a flat segment near the M point. Intercalation of hydrogen changes the number of valence electrons and shifts these bands below, reducing the complexity of the Fermi surface of $Ti_{1-x}(O_{1-x}H_x)$ as compared to that in $Ti_{1-x}O_{1-x}$ (Figure 2a and Figure 5a). In $Nb_{1-x}(O_{1-x}H_x)$, the e-ph coupling is slightly increased as compared to $Nb_{1-x}O_{1-x}$. In the former compound, the contribution at 60–70 meV is stronger and H also contributes to coupling at 110 meV. H intercalation shifts the Fermi level up and contributes to the complexity of the Fermi surface, where bands at X and Γ points and Γ–R path are closer to the Fermi level, which can promote the coupling.

The analysis of contributions to critical temperature (**Table 2**) shows that the main contribution to T_c comes from the change in the exponential factor (as one may expect). Although hydrogen intercalation boosts the ω_{log} frequency, especially in $Ti_{1-x}(O_{1-x}H_x)$, the decrease of λ overrides this beneficial effect and T_c of titanium oxide decreases. Altogether, this means that e-ph coupling strengths have the dominant influence on T_c in these oxides.

3. Conclusions

Binary oxides with the NbO-type structure can manifest strong electron-phonon coupling, as observed for $Al_{1-x}O_{1-x}$ (λ = 2.1) and $Ti_{1-x}O_{1-x}$ (λ = 1.8) in this work at x = ¼. The strength of the e-ph coupling is comparable to that reported for high-pressure, high-T_c hydrides ($\lambda \approx$ 2–3).[15,55] In $Al_{1-x}O_{1-x}$, the coupling is driven by phonon anomalies at various phonon frequencies. In $Ti_{1-x}O_{1-x}$, the coupling is primarily driven by acoustic phonons. The computationally predicted T_c reaches 36 K for $Al_{1-x}O_{1-x}$ and 35 K for $Ti_{1-x}O_{1-x}$, which is higher than in counterpart nitrides and carbides reported to date, where superconductivity also emerges from phonon mode anomalies.[33,51] The T_c and e-ph coupling are sensitive to the intercalation of hydrogen in the Ti and Nb monoxides, as it changes the number of valence electrons and thus the band structure at the Fermi level. Altogether, such intermetallic oxides with phonon anomalies are attractive for further investigation to achieve high T_c.

4. Computational Methods

Density functional theory[64,65] calculations were performed with the Quantum Espresso package.[66–68] Perdew-Burke-Ernzerhof exchange-correlation functional[69,70] and norm-conserving scalar-relativistic pseudopotentials, as provided in the PseudoDojo database (v0.4.1),[71] were employed. Planewave kinetic energy cut-off for wavefunctions was set to 90 Ry. Brillouin

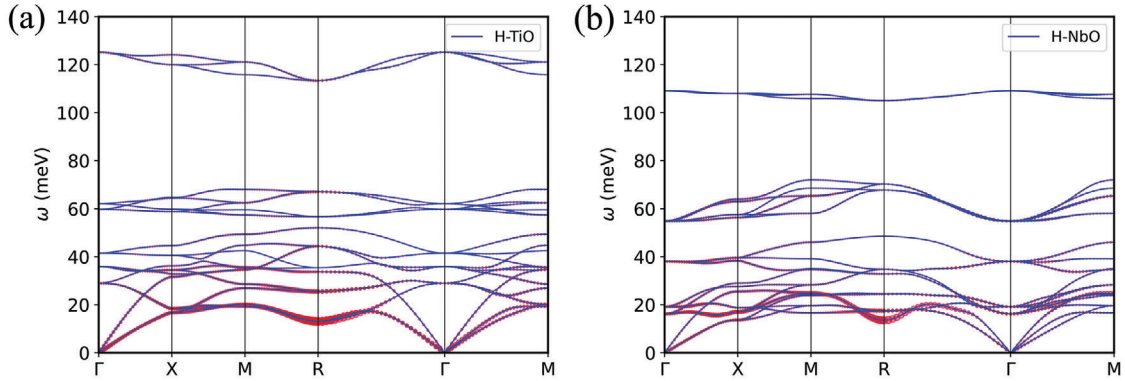

Figure 6. Phonon dispersion of *cP7* a) $Ti_{1-x}(O_{1-x}H_x)$, b) $Nb_{1-x}(O_{1-x}H_x)$ (x = ¼). Both compounds are dynamically stable (there are no imaginary frequencies). The e-ph coupling strength of each mode and q-point (λ_{qv}) is shown with red, filled circles (circle size is proportional to λ_{qv}).

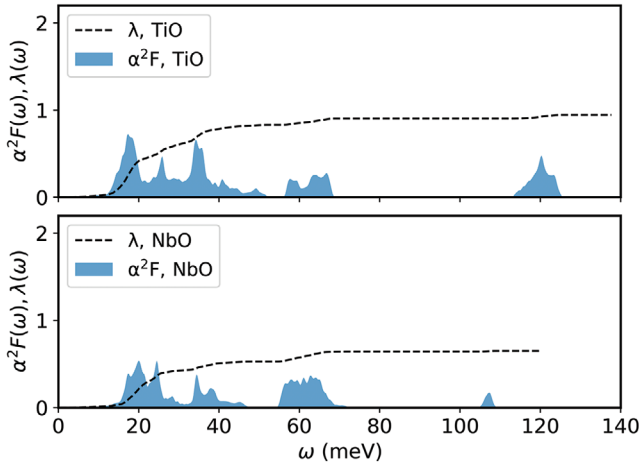

Figure 7. Eliashberg spectral function $\alpha^2F(\omega)$ and $\lambda(\omega)$ of *cP7* $Ti_{1-x}(O_{1-x}H_x)$ and $Nb_{1-x}(O_{1-x}H_x)$ ($x = 1/4$).

zone integration was performed on the Γ-centered 16 × 16 × 16 ***k***-mesh (for $Sc_{1-x}O_{1-x}$, $Ti_{1-x}O_{1-x}$, $Nb_{1-x}O_{1-x}$; for $Al_{1-x}O_{1-x}$, 20 × 20 × 20 ***k***-mesh was used). Lattice parameters and atomic positions were optimized until pressure, total energy and forces converged within 0.1 kbar, 10^{-5} Ry, and 10^{-4} Ry/Bohr, respectively (equilibrium lattice parameters are provided in Table S4, Supporting Information). The EPW code[53,72,73] was used to calculate e-ph coupling on the fine grids. The following orbitals were used for Wannier interpolation: sp^3 and d for metal atoms and sp^3 for oxygen atoms, and s orbitals for vacant sites and hydrogen. Phonon and e-ph interactions were evaluated on the coarse 6 × 6 × 6 ***q***-grid and 12 × 12 × 12 ***k***-grid. E-ph coupling and Eliashberg spectral function $\alpha^2F(\omega)$ were evaluated on the interpolated, fine 18 × 18 × 18 ***q***-grid and 36 × 36 × 36 ***k***-grid (for AlO, 24 × 24 × 24 ***q***- and 48 × 48 × 48 ***k***-grids were used). The T_c was calculated following the Allen–Dynes equation[63] with modified $f_\omega f_\mu$ prefactors that corrects predictions for high T_c superconductors:[39] $T_C^{ML} = \frac{f_\omega f_\mu \omega_{log}}{1.20}\exp(-\frac{1.04(1+\lambda)}{\lambda-\mu^*(1+0.62\lambda)})$, where $f_\omega = 1.92(\frac{\lambda+\frac{\omega_{log}}{\bar{\omega}_2}-\sqrt[3]{\mu^*}}{\sqrt{\lambda}\exp(\frac{\omega_{log}}{\bar{\omega}_2})}) - 0.08$, $f_\mu = \frac{6.86\exp(\frac{-\lambda}{\mu^*})}{\frac{1}{\lambda}-\mu^*-\frac{\omega_{log}}{\bar{\omega}_2}} + 1$, $\lambda = 2\int_0^\infty d\omega\alpha^2F(\omega)/\omega$, while $\bar{\omega}_n = \langle\omega^n\rangle^{1/n}$ and $\langle\omega^n\rangle = \frac{2}{\lambda}\int d\omega\alpha^2F(\omega)\omega^{n-1}$, and $\omega_{log} = \lim_{n\to 0}\bar{\omega}_n =$ $\exp(\frac{2}{\lambda}\int_0^\infty \frac{d\omega}{\omega}\alpha^2F(\omega)ln\omega)$;[63] μ^* was set to 0.10. Calculation of T_c^{ML} is implemented in the recent versions of the EPW code. Electron localization function[45] and Bader charges[74,75] were calculated with the VASP code[76–81] for earlier optimized structures. VESTA software was used for the visualization of crystal structure and electron localization function 2D colormaps.[82]

Table 2. Electron-phonon coupling, λ, ω_{log}, $f_\omega f_\mu/1.20$ prefactor, exponential factor ($\exp\{-1.04(1+\lambda)/[\lambda-\mu^*(1+0.62\lambda)]\}$); μ^* was set to 0.10), and critical temperature, T_c^{ML}, of $Ti_{1-x}O_{1-x}$, $Ti_{1-x}(O_{1-x}H_x$, $Nb_{1-x}O_{1-x}$, $Nb_{1-x}(O_{1-x}H_x)$. The numbers in brackets show a change of $M_{1-x}(O_{1-x}H_x)$ versus $M_{1-x}O_{1-x}$ (e.g., $\lambda_{Ti1\text{-}xO1\text{-}xHx}$ / $\lambda_{Ti1\text{-}xO1\text{-}x} \approx 0.5$).

Compound	λ	ω_{log} (meV)	$f_\omega f_\mu/1.20$ (K/meV)	exp. factor.	T_c^{ML} (K)
$Ti_{1-x}O_{1-x}$	1.80	16.8	13.0	0.16	35
$Ti_{1-x}O_{1-x}H_x$	0.96 (×0.5)	(×1.5) 25.7	(×0.8) 10.4	(×0.5) 0.08	(×0.6) 21
$Nb_{1-x}O_{1-x}$	0.47	25.4	9.8	0.011	2.8
$Nb_{1-x}O_{1-x}H_x$	0.66 (×1.4)	(×1.1) 27.1	(×1.0) 9.3	(×3.2) 0.036	(×3.3) 9.1

Supporting Information

Supporting Information is available from the Wiley Online Library or from the author.

Acknowledgements

The authors acknowledge support by NSF DMR-2132647 "EAGER: SUPER: Electrochemical Protonation to Achieve Superconducting Matter". The authors acknowledge supercomputer resources provided by the Frontera computing project DMR20012 at the Texas Advanced Computing Center. Frontera is made possible by National Science Foundation award OAC-1818253.

Conflict of Interest

The authors declare no conflict of interest.

Data Availability Statement

The data that support the findings of this study are available in the supplementary material of this article.

Keywords

BCS superconductivity, electron-phonon coupling, sub-oxides

Received: February 23, 2024
Revised: April 22, 2024
Published online:

[1] B. T. Matthias, *Rev. Mod. Phys.* **1961**, *33*, 499.
[2] T. H. Geballe, B. T. Matthias, J. P. Remeika, A. M. Clogston, V. B. Compton, J. P. Maita, H. J. Williams, *Phys. Phys. Fizika* **1966**, *2*, 293.
[3] P. W. Anderson, M. L. Cohen, in *Career in Theoretical Physics*, (2nd ed.) **2005**.
[4] L. Boeri, in *Handbook of Materials Modeling: Applications: Current and Emerging Materials*, Second Edition **2020**.
[5] M. R. Beasley, T. H. Geballe, *Phys. Today* **1984**, *37*, 347.
[6] J. Muller, *Rep. Prog. Phys.* **1980**, *43*, 641.
[7] J. G. Bednorz, K. A. Müller, *Z Phys B Con Mat* **1986**, *64*, 189 .
[8] A. Schilling, M. Cantoni, J. D. Guo, H. R. Ott, *Nature* **1993**, *363*, 56.
[9] J. Bardeen, L. N. Cooper, J. R. Schrieffer, *Phys. Rev.* **1957**, *108*, 1175.
[10] J. Nagamatsu, N. Nakagawa, T. Muranaka, Y. Zenitani, J. Akimitsu, *Nature* **2001**, *410*, 63.
[11] N. W. Ashcroft, *Phys. Rev. Lett.* **1968**, *21*, 1748.
[12] N. W. Ashcroft, *Phys. Rev. Lett.* **2004**, *92*, 187002.
[13] D. Duan, Y. Liu, F. Tian, D. Li, X. Huang, Z. Zhao, H. Yu, B. Liu, W. Tian, T. Cui, *Sci. Rep.* **2014**, *4*, 6968.

[14] D. Duan, X. Huang, F. Tian, D. Li, H. Yu, Y. Liu, Y. Ma, B. Liu, T. Cui, *Phys. Rev. B* **2015**, *91*, 180502.
[15] H. Liu, I. I. Naumov, R. Hoffmann, N. W. Ashcroft, R. J. Hemley, *Proc. Natl. Acad. Sci. USA* **2017**, *114*, 6990.
[16] F. Peng, Y. Sun, C. J. Pickard, R. J. Needs, Q. Wu, Y. Ma, *Phys. Rev. Lett.* **2017**, *119*, 107001.
[17] A. P. Drozdov, M. I. Eremets, I. A. Troyan, V. Ksenofontov, S. I. Shylin, *Nature* **2015**, *525*, 73.
[18] A. P. Drozdov, P. P. Kong, V. S. Minkov, S. P. Besedin, M. A. Kuzovnikov, S. Mozaffari, L. Balicas, F. F. Balakirev, D. E. Graf, V. B. Prakapenka, E. Greenberg, D. A. Knyazev, M. Tkacz, M. I. Eremets, *Nature* **2019**, *569*, 528.
[19] N. S. Sidorov, A. V. Palnichenko, S. S. Khasanov, *Solid State Commun.* **2010**, *150*, 1483.
[20] N. S. Sidorov, A. V. Palnichenko, S. S. Khasanov, *Solid State Commun.* **2012**, *152*, 443.
[21] A. V. Palnichenko, O. M. Vyaselev, A. A. Mazilkin, S. S. Khasanov, *Physica C* **2016**, *65*, 525.
[22] N. S. Sidorov, A. V. Palnichenko, I. I. Zver'Kova, *J. Supercond. Novel Magn.* **2010**, *24*, 1433.
[23] N. S. Sidorov, A. V. Palnichenko, S. S. Khasanov, *Physica C* **2011**, *471*, 217.
[24] A. V. Palnichenko, I. I. Zver'kova, D. V. Shakhrai, O. M. Vyaselev, *Physica C* **2019**, *558*, 25.
[25] A. V. Palnichenko, A. A. Mazilkin, O. G. Rybchenko, D. V. Shakhrai, O. M. Vyaselev, *Physica C* **2020**, *571*, 1353608.
[26] J. A. Koza, E. W. Bohannan, J. A. Switzer, *ACS Nano* **2013**, *7*, 9940.
[27] D. Wang, C. Huang, J. He, X. Che, H. Zhang, F. Huang, *ACS Omega* **2017**, *2*, 1036.
[28] G. Xu, H. Jiang, M. Stapelberg, J. Zhou, M. Liu, Q.-J. Li, Y. Cao, R. Gao, M. Cai, J. Qiao, M. S. Galanek, W. Fan, W. Xue, B. Marelli, M. Zhu, J. Li, *Environ. Sci. Technol.* **2021**, *55*, 4205.
[29] C. Zhang, F. Hao, G. Gao, X. Liu, C. Ma, Y. Lin, Y. Yin, X. Li, *npj Quantum Mater.* **2017**, *2*, 2.
[30] K. Kaminaga, D. Oka, T. Hasegawa, T. Fukumura, *J. Am. Chem. Soc.* **2018**, *140*, 6754.
[31] Y. Li, Z. Xi, Y. Wang, Z. Liu, S. Zheng, M. Liu, Z. Ma, Y. Zhang, X. Wang, H. Li, Y. Deng, Y. Yang, J.-M. Liu, D. Wu, *J. Appl. Phys.* **2023**, *134*, 235302.
[32] D. A. Papaconstantopoulos, W. E. Pickett, B. M. Klein, L. L. Boyer, *Nature* **1984**, *308*, 494.
[33] N. J. Szymanski, I. Khatri, J. G. Amar, D. Gall, S. V. Khare, *J Mater Chem C* **2019**, *7*, 12619.
[34] A. Jain, S. P. Ong, G. Hautier, W. Chen, W. D. Richards, S. Dacek, S. Cholia, D. Gunter, D. Skinner, G. Ceder, K. A. Persson, *APL Mater* **2013**, *1*, 011002.
[35] P. H. Sun, J. F. Zhang, K. Liu, Q. Han, Z. Y. Lu, *Phys. Rev. B* **2021**, *104*, 045121.
[36] W. C. Mackrodt, D. S. Middlemiss, T. G. Owens, *Phys Rev B* **2004**, *69*, 235411.
[37] M. Hoch, H. L. Johnston, *J. Am. Chem. Soc.* **1954**, *76*, 2560.
[38] G. Andersson, A. Magnéli, K. Marcker, L. G. Sillén, *Acta Chem. Scand.* **1957**, *11*, 1065.
[39] S. R. Xie, Y. Quan, A. C. Hire, B. Deng, J. M. DeStefano, I. Salinas, U. S. Shah, L. Fanfarillo, J. Lim, J. Kim, G. R. Stewart, J. J. Hamlin, P. J. Hirschfeld, R. G. Hennig, *NPJ Comput. Mater.* **2022**, *8*, 14.
[40] Https://Materialsproject.Org
[41] P. Ehrlich, *Z Elktrochem Angew P* **1939**, *45*, 362.
[42] S. Andersson, B. Collén, U. Kuylenstierna, A. Magnéli, A. Magnéli, H. Pestmalis, S. Åsbrink, *Acta Chem. Scand.* **1957**, *11*, 1641.
[43] J. K. Hulm, C. K. Jones, R. A. Hein, J. W. Gibson, *J. Low Temp. Phys.* **1972**, *7*, 291.
[44] S. V. Hosseini, M. Abbasnejad, M. R. Mohammadizadeh, *Phys. Rev. B* **2021**, *104*, 224101.
[45] B. Silvi, A. Savin, *Nature* **1994**, *371*, 683.
[46] A. P. Giddy, M. T. Dove, G. S. Pawley, V. Heine, *Acta Crystallogr. A* **1993**, *49*, 697.
[47] B. K. Greve, K. L. Martin, P. L. Lee, P. J. Chupas, K. W. Chapman, A. P. Wilkinson, *J. Am. Chem. Soc.* **2010**, *132*, 15496.
[48] B. T. Matthias, *Phys. Rev.* **1955**, *97*, 74.
[49] W. L. McMillan, *Phys. Rev.* **1968**, *167*, 331.
[50] E. E. Havinga, H. Damsma, M. H. Van Maaren, *J. Phys. Chem. Solids* **1970**, *31*, 2653.
[51] E. I. Isaev, S. I. Simak, I. A. Abrikosov, R. Ahuja, Y. K. Vekilov, M. I. Katsnelson, A. I. Lichtenstein, B. Johansson, *J. Appl. Phys.* **2007**, *101*, 123519.
[52] C. Kokail, C. Heil, L. Boeri, *Phys. Rev. B* **2016**, *94*, 060502.
[53] E. R. Margine, F. Giustino, *Phys. Rev. Bt* **2013**, *87*, 024505.
[54] G. P. Kafle, C. R. Tomassetti, I. I. Mazin, A. N. Kolmogorov, E. R. Margine, *Phys. Rev. Mater.* **2022**, *6*, 084801.
[55] I. Errea, M. Calandra, C. J. Pickard, J. Nelson, R. J. Needs, Y. Li, H. Liu, Y. Zhang, Y. Ma, F. Mauri, *Phys. Rev. Lett.* **2015**, *114*, 157004.
[56] K. Dolui, L. J. Conway, C. Heil, T. A. Strobel, R. Prasankumar, C. J. Pickard, *Phys. Rev. Lett.* **2024**, *132*, 166001.
[57] R. Vocaturo, C. Tresca, G. Ghiringhelli, G. Profeta, *J. Appl. Phys.* **2022**, *131*, 033903.
[58] M. D. Banus, T. B. Reed, A. J. Strauss, *Phys. Rev. B* **1972**, *5*, 2775.
[59] N. J. Doyle, J. K. Hulm, C. K. Jones, R. C. Miller, A. Taylor, *Phys. Lett. A* **1968**, *26*, 604.
[60] B. Rousseau, A. Bergara, *Phys. Rev. B* **2010**, *82*, 104504.
[61] I. A. Troyan, D. V. Semenok, A. G. Kvashnin, A. V. Sadakov, O. A. Sobolevskiy, V. M. Pudalov, A. G. Ivanova, V. B. Prakapenka, E. Greenberg, A. G. Gavriliuk, I. S. Lyubutin, V. V. Struzhkin, A. Bergara, I. Errea, R. Bianco, M. Calandra, F. Mauri, L. Monacelli, R. Akashi, A. R. Oganov, *Adv. Mater.* **2021**, *33*, 2006832.
[62] Z. P. Yin, A. Kutepov, G. Kotliar, *Phys. Rev. X* **2013**, *3*, 021011.
[63] P. B. Allen, R. C. Dynes, *Phys. Rev. B* **1975**, *12*, 905.
[64] P. Hohenberg, W. Kohn, *Phys. Rev.* **1964**, *136*, B864.
[65] W. Kohn, L. J. Sham, *Phys. Rev.* **1965**, *140*, A1133.
[66] P. Giannozzi, et al., *J. Phys.: Condens. Matter* **2009**, *21*, 395502.
[67] P. Giannozzi, et al., *J. Phys.: Condens. Matter* **2017**, *29*, 465901.
[68] P. Giannozzi, O. Baseggio, P. Bonfà, D. Brunato, R. Car, I. Carnimeo, C. Cavazzoni, S. de Gironcoli, P. Delugas, F. Ferrari Ruffino, A. Ferretti, N. Marzari, I. Timrov, A. Urru, S. Baroni, *J. Chem. Phys.* **2020**, *152*, 154105.
[69] J. P. Perdew, K. Burke, M. Ernzerhof, *Phys. Rev. Lett.* **1996**, *77*, 3865.
[70] J. P. Perdew, K. Burke, M. Ernzerhof, *Phys. Rev. Lett.* **1997**, *78*, 1396.
[71] M. J. van Setten, M. Giantomassi, E. Bousquet, M. J. Verstraete, D. R. Hamann, X. Gonze, G. M. Rignanese, *Comput. Phys. Commun.* **2018**, *226*, 39.
[72] F. Giustino, M. L. Cohen, S. G. Louie, *Phys. Rev. B* **2007**, *76*, 165108.
[73] S. Poncé, E. R. Margine, C. Verdi, F. Giustino, *Comput. Phys. Commun.* **2016**, *209*, 116.
[74] R. F. W. Bader, *Atoms in Molecules: A Quantum Theory* (Clarendon Press, **1990**).
[75] W. Tang, E. Sanville, G. Henkelman, *J. Phys. Condens. Matter* **2009**, *21*, 084204.
[76] G. Kresse, J. Furthmüller, *Phys. Rev. B* **1996**, *54*, 11169.
[77] G. Kresse, J. Furthmüller, *Comput. Mater. Sci.* **1996**, *6*, 15.
[78] G. Kresse, J. Hafner, *Phys. Rev. B* **1994**, *49*, 14251.
[79] G. Kresse, J. Hafner, *Phys. Rev. B* **1993**, *47*, 558.
[80] P. E. Blöchl, *Phys. Rev. B* **1994**, *50*, 17953.
[81] D. Joubert, *Phys. Rev. B* **1999**, *59*, 1758.
[82] K. Momma, F. Izumi, *J. Appl. Crystallogr.* **2011**, *44*, 1272.

ADVANCED ELECTRONIC MATERIALS
Open Access

Supporting Information

for *Adv. Electron. Mater.*, DOI 10.1002/aelm.202400141

Superconductivity and Pronounced Electron-Phonon Coupling in Rock-Salt $Al_{1-x}O_{1-x}$ and $Ti_{1-x}O_{1-x}$

Pjotrs Žguns, Nuh Gedik, Bilge Yildiz and Ju Li**

Supporting Information

Superconductivity and Pronounced Electron-Phonon Coupling in Rock-Salt $Al_{1-x}O_{1-x}$ and $Ti_{1-x}O_{1-x}$

Pjotrs Žguns[1], Nuh Gedik[2], Bilge Yildiz[1,3,*] and Ju Li[1,3,*]

[1] Department of Materials Science and Engineering, Massachusetts Institute of Technology, 77 Massachusetts Avenue, Cambridge, MA 02139-4307, USA
[2] Department of Physics, 77 Massachusetts Avenue, Cambridge, MA 02139-4307, USA
[3] Department of Nuclear Science and Engineering, Massachusetts Institute of Technology, 77 Massachusetts Avenue, Cambridge, MA 02139-4307, USA

[*]To whom correspondence should be addressed: byildiz@mit.edu, liju@mit.edu

Table S1. Phase stability of $Al_{1-x}O_{1-x}$, $Sc_{1-x}O_{1-x}$, $Ti_{1-x}O_{1-x}$, $Nb_{1-x}O_{1-x}$ in two structures: the rock-salt structure (B1, *cP*8, $x = 0$) and rock-salt structure with vacancies ($x = ¼$, *cP*6, NbO-type [1]). E^{MP}_{hull} is the energy above the convex hull as reported in the Materials Project database [2]. ΔE is the energy difference between the *cP*6 and *cP*8 structures as calculated in this work (eV/atom): $\Delta E = ⅙ E_{cP6} - ⅛ E_{cP8}$. $E_{hull,\ cP6}$ is the energy above the convex hull of the *cP*6 structure calculated as follows: $E_{hull,\ cP6} = E^{MP}_{hull,\ cP8} + \Delta E$. All MP structures are non-magnetic except mp-755300 ($Ti_{1-x}O_{1-x}$, $x = ¼$, *cP*6), which is ferromagnetic.

	B1 structure MP	NbO structure MP	NbO structure this work	B1 → NbO this work
	$E^{MP}_{hull,\ cP8}$ (eV/atom)	$E^{MP}_{hull,\ cP6}$ (eV/atom)	$E_{hull,\ cP6}$ (eV/atom)	ΔE (eV/atom)
$Al_{1-x}O_{1-x}$	1.303 mp-8023	n/a	0.768	−0.535
$Sc_{1-x}O_{1-x}$	0.104 mp-644481	n/a	0.433	0.329
$Ti_{1-x}O_{1-x}$	0.272 mp-2664	0.113 mp-755300	0.098	−0.174
$Nb_{1-x}O_{1-x}$	0.789 mp-2692	0.000 mp-2311	−0.006	−0.795

Table S2. The Bader charges of $M_{1-x}O_{1-x}$ (*cP*6, x = ¼; NbO-type structure). q_M and q_O are the Bader charges of, respectively, metal and oxygen atoms. q_{VM} and q_{VO} are the Bader charges of, respectively, metal and oxygen vacancies located at, respectively, (0, 0, 0) and (½, ½, ½) sites.

Compound	q_M	q_O	q_{VM}	q_{VO}
$Al_{1-x}O_{1-x}$	+1.72	−1.72	0.00	0.00
$Sc_{1-x}O_{1-x}$	+1.49	−1.72	0.00	−0.52
$Ti_{1-x}O_{1-x}$	+1.28	−1.28	0.00	0.00
$Nb_{1-x}O_{1-x}$	+1.20	−1.20	0.00	0.00

Table S3. Hydrogen intercalation energy, ΔE_{int}, *vs*. hydrogen gas molecule (H_2) and *vs*. solid PdH_x. ΔE_{int}, = $E(HM_3O_3) - E(M_3O_3) - ½\ E(H_2)$. List of computational parameters. N_{at}, the number of atoms. Two intercalation sites were considered: the metal vacancy site, and the oxygen vacancy site. Electron-phonon coupling, λ, and T_c^{ML} were calculated for dynamically stable compounds.

Compound	ΔE_{int} *vs*. H_2 (eV)	ΔE_{int} *vs*. PdH_x (eV)	Phonon stability	λ	T_c^{ML} (K)
H on metal site					
$Al_{1-x}H_xO_{1-x}$	3.40	3.59	Unstable	n/a	n/a
$Sc_{1-x}H_xO_{1-x}$	2.71	2.90	Unstable	n/a	n/a
$Ti_{1-x}H_xO_{1-x}$	3.05	3.24	Unstable	n/a	n/a
$Nb_{1-x}H_xO_{1-x}$	3.34	3.53	Unstable	n/a	n/a
H on oxygen site					
$Al_{1-x}O_{1-x}H_x$	1.33	1.52	Unstable	n/a	n/a
$Sc_{1-x}O_{1-x}H_x$	−0.25	−0.06	Unstable	n/a	n/a
$Ti_{1-x}O_{1-x}H_x$	−0.77	−0.58	Stable	0.96	21
$Nb_{1-x}O_{1-x}H_x$	−0.21	−0.02	Stable	0.66	9

Table S4. List of computational parameters of $M_{1-x}O_{1-x}$ compounds for both x = 0, *cP*8, and x = ¼, *cP*6. E_{cut}, the plane-wave energy cut-off. N_i, the subdivision of the *k*-point mesh (Γ-centered). The resultant, optimized lattice constants are provided.

Compound	Pearson symbol	E_{cut} (Ry)	$N_1 \times N_2 \times N_3$	Lattice constant (Å)
$Al_{1.00}O_{1.00}$	*cP*8	90	17 × 17 × 17	4.473
$Al_{0.75}O_{0.75}$	*cP*6	90	20 × 20 × 20	3.951
$Sc_{1.00}O_{1.00}$	*cP*8	90	20 × 20 × 20	4.467
$Sc_{0.75}O_{0.75}$	*cP*6	90	14 × 14 × 14	4.328
$Ti_{1.00}O_{1.00}$	*cP*8	90	20 × 20 × 20	4.278
$Ti_{0.75}O_{0.75}$	*cP*6	90	16 × 16 × 16	4.077
$Nb_{1.00}O_{1.00}$	*cP*8	90	22 × 22 × 22	4.472
$Nb_{0.75}O_{0.75}$	*cP*6	90	16 × 16 × 16	4.233

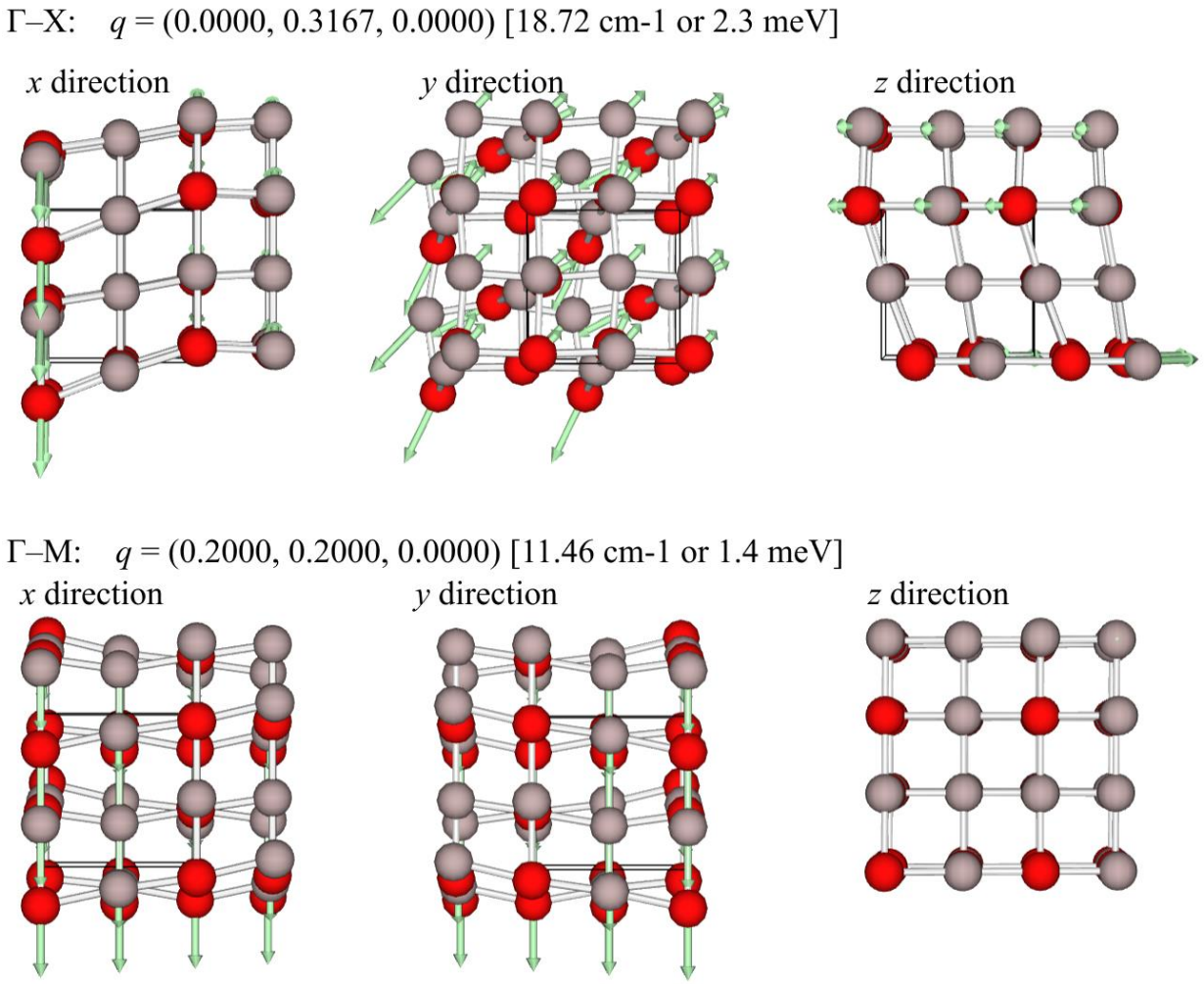

Fig. S1. Snapshots of $Al_{1-x}O_{1-x}$ phonon modes at the Γ–X and Γ–M edges, that show pronounced e-ph coupling (see Fig. 3a). Color code: Al is grey, O is red. Prepared with the interactive phonon visualizer at Materials Cloud [3].

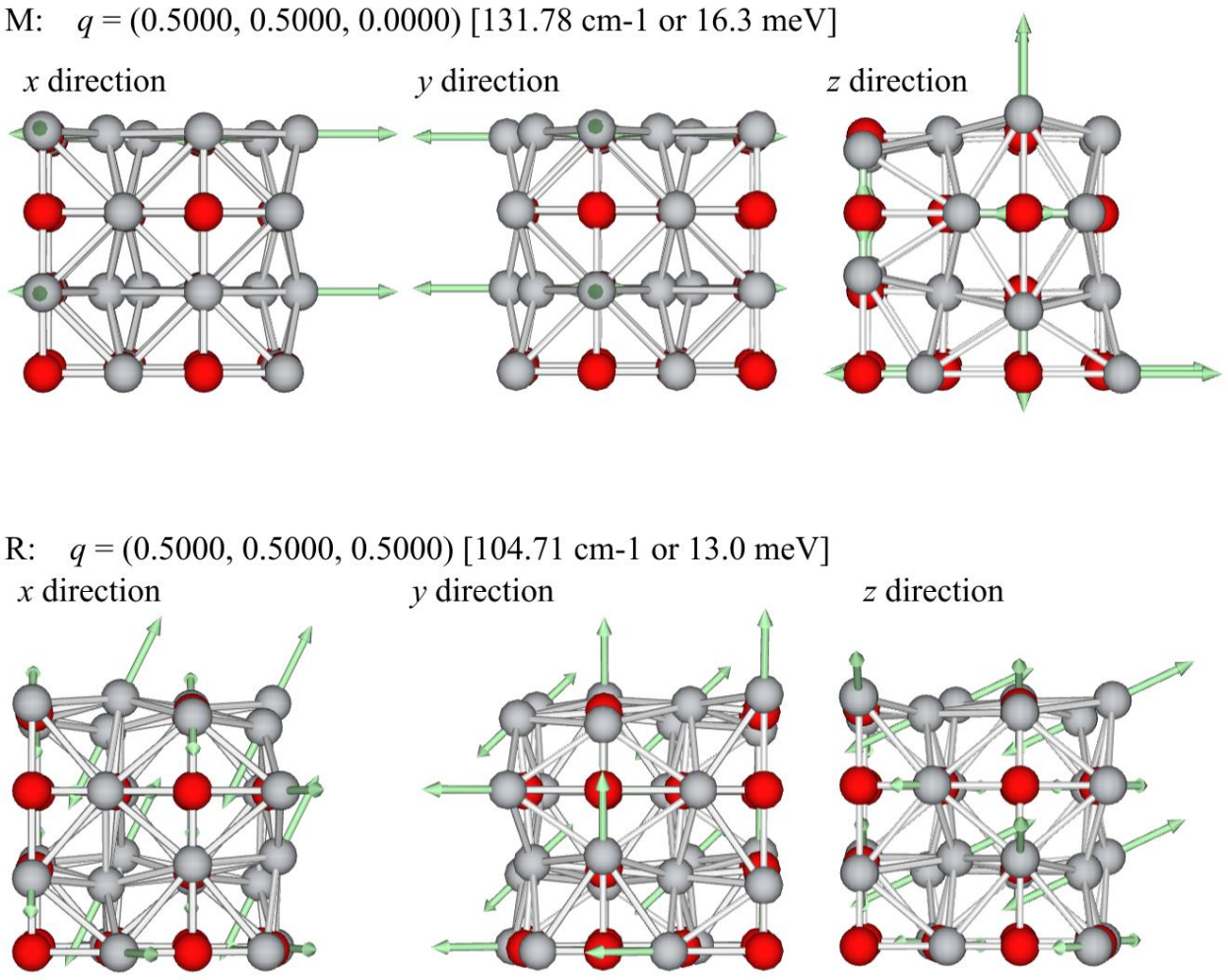

Fig. S2. Snapshots of $Ti_{1-x}O_{1-x}$ phonon modes at M and R points, that show pronounced e-ph coupling (see Fig. 3c). Color code: Ti is grey, O is red. Prepared with the interactive phonon visualizer at Materials Cloud [3].

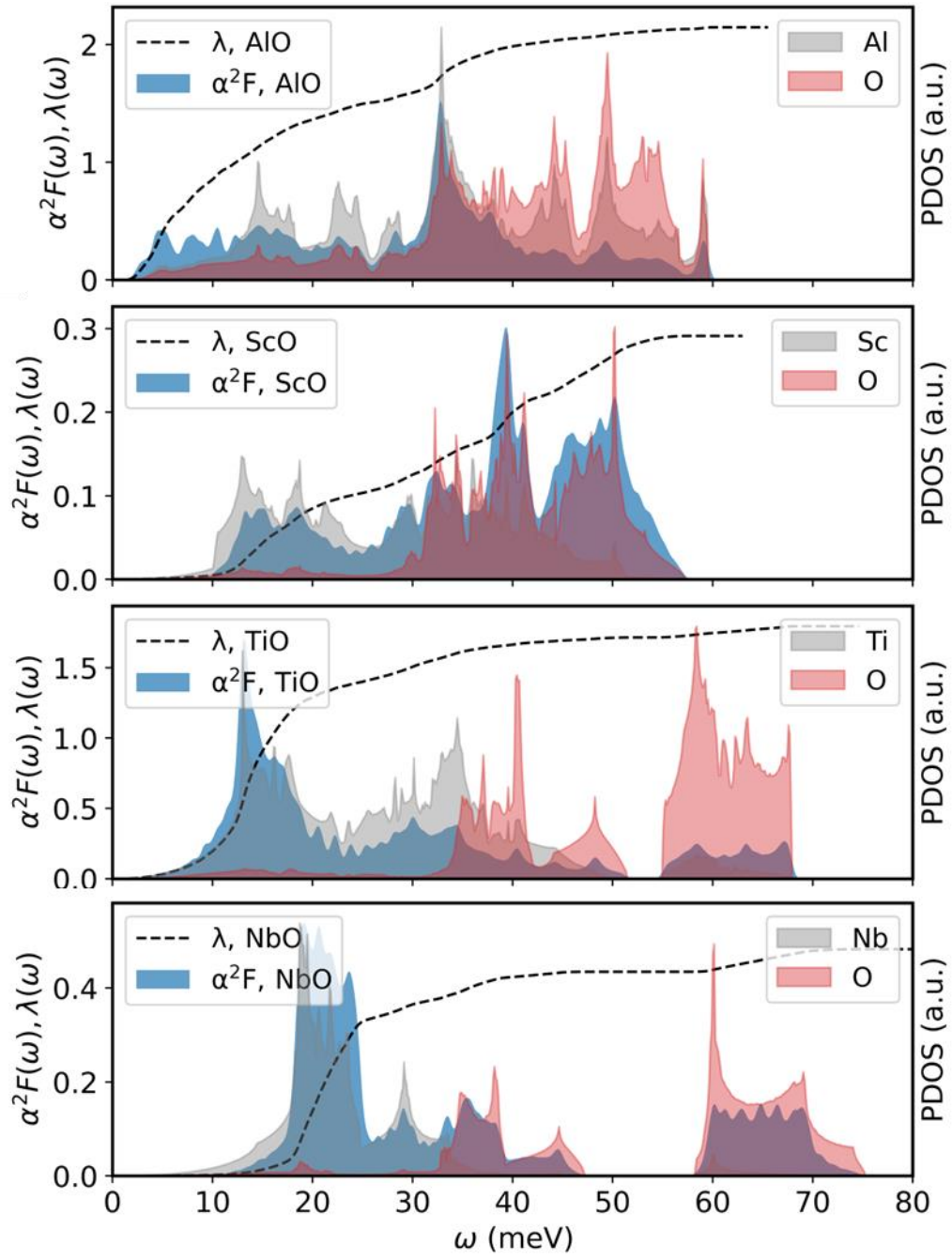

Fig. S3. Eliashberg spectral function $\alpha^2F(\omega)$ and $\lambda(\omega)$ of $Al_{1-x}O_{1-x}$, $Sc_{1-x}O_{1-x}$, $Ti_{1-x}O_{1-x}$, and $Nb_{1-x}O_{1-x}$ (x = ¼, *cP*6, NbO-type structure). The phonon DOS (PDOS) projected onto metal (grey) and oxygen (red) atoms is also shown.

References:

[1] G. Andersson, A. Magnéli, K. Marcker, and L. G. Sillén, *Note on the Crystal Structure of Niobium Monoxide.,* Acta Chem Scand **11**, (1957).

[2] A. Jain et al., *Commentary: The Materials Project: A Materials Genome Approach to Accelerating Materials Innovation,* APL Mater **1**, 011002 (2013).

[3] L. Talirz et al., *Materials Cloud, a Platform for Open Computational Science,* Sci Data **7**, (2020).